engineering proceedings

Proceeding Paper

Metaheuristic-Based Photovoltaic Parameter Identification Using a Dynamic Elite Cooperative Artificial Circulatory System Algorithm †

Nermin Özcan [1,*] and Imam Barket Ghiloubi [2]

[1] Department of Biomedical Engineering, Faculty of Engineering and Natural Sciences, Iskenderun Technical University, 31200 İskenderun, Hatay, Türkiye
[2] Identification, Command, Control & Communication Laboratory, Mohamed Khider University, Biskra 07000, Algeria; imam.ghiloubi@univ-biskra.dz
* Correspondence: nermin.ozcan@iste.edu.tr
† Presented at the 1st International Online Conference on Inventions - Energy Security and Sustainable Development, 25–26 June 2026; Available online: https://sciforum.net/event/IOCIV2026.

Abstract

Accurate parameter estimation of photovoltaic (PV) models is essential for performance evaluation, efficiency enhancement, and reliable energy forecasting in solar energy systems. However, the nonlinear, multimodal, and implicit nature of the current–voltage (I–V) relationship makes this task challenging for conventional optimization methods, which often suffer from premature convergence and sensitivity to initial conditions. In this study, a modified variant of the Artificial Circulatory System Algorithm, termed Dynamic Elite Cooperative ACSA (DEC-ACSA), is proposed for estimating the unknown parameters of the Single-Diode Model (SDM). The proposed approach extends the original ACSA by incorporating dynamic population grouping, elite-guided cooperative interaction, and directional elite refinement, thereby aiming to improve convergence stability and the utilization of high-quality population information. The objective is to minimize the residual root mean square error (RMSE) of the implicit SDM equation using measured I–V data from four established benchmarks: the RTC France solar cell and the PWP201, STM6-40/36, and STP6-120/36 PV modules. The performance of DEC-ACSA is evaluated against the original ACSA, Particle Swarm Optimization (PSO), Grey Wolf Optimizer (GWO), Genetic Algorithm (GA), and Henry Gas Solubility Optimization (HGSO) over 30 independent runs under an equal budget of 50,100 function evaluations. The DEC-ACSA configuration selected on RTC France was retained unchanged for the three additional module benchmarks. DEC-ACSA achieved mean residual RMSE values of 1.2514×10^{-3}, 2.656×10^{-3}, 2.647×10^{-3}, and 1.8108×10^{-2} for RTC France, PWP201, STM6-40/36, and STP6-120/36, respectively, while consistently reducing run-to-run variability relative to ACSA. Holm-corrected tests showed no significant difference from PSO on RTC France and PWP201, whereas significant differences from all comparison algorithms were observed on STM6-40/36 and STP6-120/36. I–V reconstruction further confirmed close agreement with the measured data across all four PV systems.

Keywords: Artificial Circulatory System Algorithm; photovoltaic parameter estimation; metaheuristic optimization; Single-Diode Model

Check for updates

Academic Editor: Eugen Rusu

Published: 2 September 2026

Copyright: © 2026 by the authors. Licensee MDPI, Basel, Switzerland. This article is an open access article distributed under the terms and conditions of the Creative Commons Attribution (CC BY) license.

1. Introduction

The increasing demand for clean and sustainable energy has accelerated the deployment of photovoltaic (PV) systems worldwide. As PV installations continue to expand from residential applications to utility-scale power plants, accurate modeling of photovoltaic cells and modules has become increasingly important for system design, performance evaluation, maximum power point tracking, fault diagnosis, and energy management. Since the electrical characteristics of PV devices are highly nonlinear and strongly affected by environmental conditions such as solar irradiance and temperature, reliable mathematical models are essential for accurately predicting their operating behavior [1]. Recent studies further emphasize that reliable parameter identification directly affects the fidelity of I–V characteristics and, consequently, the accuracy of PV performance prediction and optimization [2,3].

Among the various equivalent circuit models, the Single-Diode Model (SDM) has become the most widely adopted because it provides an effective balance between modeling accuracy and computational complexity. The SDM represents the electrical behavior of a PV cell using five unknown parameters, namely the photocurrent, reverse saturation current, series resistance, shunt resistance, and diode ideality factor. However, estimating these parameters remains a challenging optimization problem because the governing current–voltage equation is nonlinear, implicit, and highly coupled [4]. PV parameter-estimation methods can be broadly categorized into analytical, deterministic numerical, metaheuristic, or hybrid approaches. Analytical techniques can provide computationally efficient solutions but often rely on simplifying assumptions, whereas iterative deterministic methods may exhibit sensitivity to initialization and numerical convergence when highly nonlinear PV equations are considered [3,5]. Furthermore, the formulation of the objective function and the numerical procedure used to obtain the estimated current can substantially influence the resulting parameter estimates [6].

Population-based metaheuristic optimization algorithms have attracted considerable attention for photovoltaic parameter identification due to their ability to effectively solve nonlinear, multimodal optimization problems. Classical methods such as Particle Swarm Optimization, Differential Evolution, and Genetic Algorithms have been extensively studied, while more recent approaches including Grey Wolf Optimizer, Jaya algorithm, Teaching–Learning-Based Optimization, and Whale Optimization Algorithm have demonstrated competitive estimation accuracy [7]. These derivative-free algorithms are capable of handling the nonlinear and multimodal nature of the parameter estimation problem without requiring explicit mathematical reformulation. Recent research indicates that the field has increasingly shifted from the direct application of standard optimizers toward modified, hybrid, and search-enhanced variants. For example, Almodfer (2022) [8] incorporated chaotic dynamics into the Honey Badger Algorithm to improve its search capability, while Rathod (2024) [9] combined the Pelican Optimization Algorithm with a Newton–Raphson procedure for SDM parameter extraction. Bennagi (2025) [10] proposed a PID-based search framework incorporating a Lévy-flight-based mechanism to improve search diversity and mitigate local-optimum entrapment, whereas Almabrouk (2026) [11] hybridized the Bat and Crow Search algorithms to combine global exploration with local exploitation. More recently, Tanguturi (2026) [3] combined chaos-enhanced global exploration with adaptive deterministic refinement to improve convergence stability and numerical robustness. These studies demonstrate that improving search reliability and convergence behavior, rather than merely introducing additional optimizers, remains an active research direction in PV parameter identification.

Although recent studies have significantly improved estimation accuracy, maintaining an effective balance between exploration and exploitation remains a fundamental

challenge. During the optimization process, many population-based algorithms gradually lose population diversity as search agents converge toward a limited region of the search space. Existing studies have attempted to alleviate these limitations through mechanisms such as chaotic search strategies, Lévy-flight-based operators, and adaptive or trigonometric search enhancements [12–14]. Other studies have employed ranking mechanisms, directional population information, multiple-population structures, and elite-guided refinement to improve the utilization of high-quality search information. For instance, Abdel-Basset (2021) [15] incorporated a ranking-based updating mechanism into GNDO to improve population-information utilization and alleviate premature convergence. Almutairi (2025) [5] reviewed population-diversification approaches based on multiple initial populations and subsequent elite-pool formation, while Almutairi (2026) [16] applied quadratic-interpolation refinement to a subset of elite individuals to enhance local search and convergence accuracy. These developments clearly indicate that elite-guided, ranking-based, and cooperative population-information mechanisms are established concepts in metaheuristic optimization. Therefore, the research gap considered in this study is not the absence of elite cooperation itself, but rather the opportunity to adapt such information-utilization mechanisms to the specific search structure of the recently proposed Artificial Circulatory System Algorithm (ACSA) [17]. In particular, the baseline ACSA may exhibit considerable run-to-run variation, while its original population-update structure does not explicitly incorporate a dynamic mechanism for exploiting information distributed among a set of high-quality solutions. This motivates an ACSA-specific modification aimed at improving convergence stability and robustness without replacing its underlying physiological search framework.

Motivated by this observation, this paper proposes a Dynamic Elite Cooperative Artificial Circulatory System Algorithm (DEC-ACSA) for photovoltaic parameter identification. Unlike the original ACSA, the proposed approach integrates a Dynamic Elite Cooperative framework into the ACSA search process with the primary objective of improving its convergence stability and robustness across independent optimization runs. The proposed framework combines dynamic population grouping with elite-guided cooperative interaction and elite-based search refinement, allowing information from high-quality solutions to be utilized more systematically during the search process. Instead of relying solely on the globally best individual, the proposed search structure is designed to maintain a more effective balance between population diversity and exploitation of promising regions. It should be emphasized that elite-guided and cooperative search are established concepts in metaheuristic optimization; therefore, the contribution of this study does not lie in introducing elite cooperation itself, but in its integration and adaptation within the specific search structure of ACSA to address the convergence variability observed in the baseline algorithm. The proposed approach is evaluated on four established SDM benchmarks comprising the RTC France solar cell [18] and the PWP201, STM6-40/36, and STP6-120/36 PV modules. This extended validation covers different PV devices and operating temperatures, enabling the robustness and transferability of DEC-ACSA to be assessed beyond a single benchmark. DEC-ACSA is evaluated against the original ACSA and established population-based metaheuristic algorithms under an equal function-evaluation budget, with particular emphasis on parameter-estimation accuracy, convergence behavior, run-to-run stability, parameter sensitivity, and computational cost. The parameter configuration selected through sensitivity analysis on the RTC France benchmark is retained unchanged for the additional PV module benchmarks to avoid benchmark-specific retuning and to provide a more stringent assessment of the method across different PV systems.

2. Methodology

2.1. Single-Diode Model

The electrical behavior of a PV cell can be accurately represented using equivalent circuit models. Among these, the SDM is widely adopted because it provides an effective compromise between modeling accuracy and computational complexity. The SDM consists of a photocurrent source, a diode, a series resistance (R_s), and a shunt resistance (R_{sh}), resulting in a nonlinear implicit current–voltage relationship, as illustrated in Figure 1.

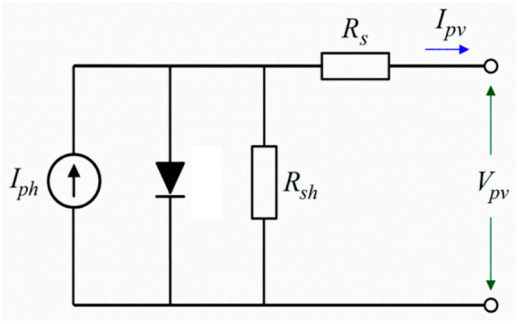


Figure 1. Single-Diode Model (SDM) equivalent circuit used for photovoltaic parameter estimation.

The output current of the SDM is expressed as:

$$I = I_{ph} - I_{s(\exp(\frac{V + I R_s}{n V_t}) - 1)} - \frac{V + I R_s}{R_{sh}} \quad (1)$$

where I_{ph}, I_s, R_s, R_{sh}, and n denote the photocurrent, reverse saturation current, series resistance, shunt resistance, and diode ideality factor, respectively. The thermal voltage is defined as $V_t = kT/q$, where k is the Boltzmann constant, T is the cell temperature in Kelvin, and q is the elementary charge. Equation (1) describes the SDM at the cell level. For PV modules consisting of N_s series-connected and N_p parallel-connected cells, the corresponding cell-equivalent voltage is defined as:

$$V_c = \frac{V}{N_s} + \frac{IR_s}{N_p} \quad (2)$$

and the corresponding module current is expressed as:

$$I = N_p \left[I_{ph} - I_s \left(\exp\left(\frac{qV_c}{nkT} \right) - 1 \right) \right] - \frac{V_c}{R_{sh}} \quad (3)$$

Equations (2) and (3) reduce to the single-cell formulation in Equation (1) when $N_s = N_p = 1$. This formulation allows the same five per-cell SDM parameters to be estimated consistently for both the RTC France solar cell and the additional series-connected PV module benchmarks.

Accordingly, the parameter estimation problem is formulated as a five-dimensional optimization problem,

$$\boldsymbol{X} = \left[I_{ph}, I_s, R_s, R_{sh}, n \right] \quad (4)$$

The objective of the optimization process is to minimize the discrepancy between the experimentally measured current and the current–voltage relationship defined by the SDM. For each measured pair (V_i,I_i^{exp}), the cell-equivalent voltage is first calculated according to Equation (2), and the residual of the implicit SDM equation is defined as:

https://doi.org/10.3390/engproc2026152004

$$r_i(\mathbf{X}) = I_{ph} - I_s \left[\exp\left(\frac{q\left(V_i + I_i^{exp} R_s\right)}{nkT} \right) - 1 \right] - \frac{V_i + I_i^{exp} R_s}{R_{sh}} - I_i^{exp} \quad (5)$$

The residual RMSE is then adopted as the objective function:

$$f(\mathbf{X}) = \sqrt{\frac{1}{N} \sum_{i=1}^{N} r_i(\mathbf{X})^2} \quad (6)$$

where (N) denotes the number of measured I–V data points. The optimization problem is therefore formulated as the minimization of $f(\mathbf{X})$ in Equation (6), subject to the predefined lower and upper bounds of the five SDM parameters in Equation (4). For the post-optimization evaluation of the identified parameters, the implicit SDM equation given by Equations (2) and (3) is numerically solved to obtain the estimated current values, from which the corresponding I–V prediction errors are calculated. In the Section 3, the parameters defined in Equation (4) are reported for each PV benchmark, while the residual RMSE in Equation (6) is used as the optimization-performance criterion and the reconstructed I–V curves obtained from Equations (2) and (3) are used to assess the physical agreement between the identified model and the measured data.

2.2. Artificial Circulatory System Algorithm

The Artificial Circulatory System Algorithm (ACSA) is a recently proposed bio-inspired optimization algorithm motivated by the regulatory mechanisms of the human circulatory system [17]. The algorithm mimics the coordinated regulation of blood circulation through physiological feedback mechanisms to achieve a balance between global exploration and local exploitation during the optimization process.

Initially, candidate solutions are randomly distributed within the search space. During each iteration, their positions are updated according to the adaptive search strategy defined in the original ACSA, allowing the population to gradually move toward promising regions while maintaining exploration capability. The search process alternates between exploratory and exploitative behaviors according to the algorithm's adaptive control mechanism. Additional details regarding the mathematical formulation of the original ACSA can be found in the original publication.

Although ACSA demonstrates competitive optimization performance, its search process is primarily guided by the best-performing individuals. Consequently, useful information obtained by other high-quality solutions may not be sufficiently utilized, which can reduce population diversity during the later stages of optimization. Moreover, the substantial run-to-run variability observed in the baseline ACSA motivates the development of a more structured mechanism for controlling population diversity and utilizing information from high-quality solutions. Accordingly, DEC-ACSA retains the fundamental physiological search framework of ACSA while modifying its population grouping and information-sharing mechanisms.

2.3. Dynamic Elite Cooperative Strategy

To overcome the above limitation, a Dynamic Elite Cooperative Strategy is incorporated into the original ACSA framework. The proposed DEC-ACSA extends the original search structure through three interconnected mechanisms: (i) diversity-aware dynamic population grouping, (ii) stochastic elite-guided cooperative interaction, and (iii) directional elite refinement. The mathematical roles of the associated control parameters are specified in Equations (7)–(16), and their relationship with the parameter-sensitivity analysis and the subsequent multi-benchmark evaluation is described in Section 3.

2.3.1. Diversity-Aware Dynamic Population Grouping

At each search cycle, the population is ranked according to fitness and dynamically partitioned into neural, hormonal, and elite groups. The grouping mechanism considers both optimization progress and current population diversity. The normalized search progress is defined as:

$$p = \frac{N_{FE}}{N_{FE}^{max}} \tag{7}$$

where N_{FE} and $N_{FE}{}^{max}$ denote the current and maximum numbers of function evaluations, respectively. Thus, the progress variable p in Equation (7) directly controls the stage-dependent group ratios and the elite-refinement coefficient defined below.

Population diversity is estimated using the normalized standard deviation of the decision variables:

$$D = \text{clip}\left[\frac{1}{D_0}\left(\frac{1}{d}\sum_{j=1}^{d}\frac{\sigma_j}{UB_j - LB_j}\right), 0, 1\right] \tag{8}$$

where d is the problem dimension, σ_j is the population standard deviation of the *jth* decision variable, UB_j and LB_j denote its upper and lower bounds, respectively, and D_0 = 0.289 is used as the normalization factor. The diversity measure D in Equation (8) is subsequently used in Equation (9) to adapt the neural-group proportion when population diversity decreases.

The proportion assigned to the neural group is dynamically determined by:

$$r_N = \text{clip}\left[r_N^{max} - \left(r_N^{max} - r_N^{min}\right)p + \lambda_D(1 - D),\ r_N^{min},\ 0.45\right] \tag{9}$$

where r_N^{min} and r_N^{max} define the allowable neural-group ratio and λ_D controls the influence of diversity term. Thus, the neural proportion generally decreases with optimization progress but can increase when population diversity becomes low.

The elite ratio changes progressively according to:

$$r_E = r_E^{min} + \left(r_E^{max} - r_E^{min}\right)p \tag{10}$$

After ranking the population from the worst to the best solution, the lowest-ranked N_N individuals form the neural group, the highest-ranked N_E individuals constitute the elite set, and the remaining solutions form the hormonal group, where:

$$N_N = \text{round}(Nr_N), \qquad N_E = \text{round}(Nr_E) \tag{11}$$

This adaptive partitioning links the population structure to both the stage of the optimization process and the observed loss of population diversity. Accordingly, Equations (7)–(11) determine the neural and elite subsets used by the search updates in Sections 2.3.2–2.3.4.

2.3.2. Neural and Hormonal Search Updates

The neural group primarily maintains exploratory search behavior. The DEC-ACSA generates the neural candidate using a stimulation-scaled population difference:

$$\mathbf{x}_i^N = \mathbf{x}_i + \mathbf{a} \odot \mathbf{s}_i^N \odot (\mathbf{x}_{r_1} - \mathbf{x}_{r_2}) \tag{12}$$

where r_1 and r_2 are two distinct randomly selected population indices, a is a random vector with components sampled from [0.5, 1], $\odot$ denotes element-wise multiplication, and $s_i{}^N$ is the normalized neural stimulation vector inherited from the ACSA stimulation mechanism.

The candidate in Equation (12) therefore provides the exploratory update for individuals assigned to the neural group by Equation (11).

For hormonal-group individuals that are not subjected to cooperative guidance, the original hormonal search principle is retained in modified form. Depending on a random decision, a candidate is generated either through a bounded hormonal stimulation around the current solution or through a population-direction update involving the population mean and a difference vector between two randomly selected solutions.

2.3.3. Elite-Guided Cooperative Interaction

After the neural-group update, the population is re-evaluated and the elite set is refreshed. For each hormonal individual, elite-guided cooperation is applied with probability P_c. When cooperation is selected, one solution x_e is randomly sampled from the current elite set and the cooperative candidate is generated as:

$$\mathbf{x}_i^C = \mathbf{x}_i + \mathbf{r} \odot (\mathbf{x}_e - \mathbf{x}_i) \tag{13}$$

where $\mathbf{r}$ is a random vector uniformly distributed in $[0, 1]^d$. This operator moves the current solution toward a randomly selected high-quality solution rather than deterministically following only the global best. Because the guiding elite is sampled from a dynamically updated elite pool, different high-quality search regions can influence the hormonal population throughout the optimization process. The cooperation probability *Pc* in Equation (11) is one of the principal DEC-ACSA control parameters examined in the sensitivity analysis in Section 3.2.

2.3.4. Directional Elite Refinement

The elite solutions themselves are subsequently refined using information from the current global best, directional differences within the elite set, and the weighted elite centroid. For an elite solution x_i, the candidate is generated as:

$$\mathbf{x}_i^E = \mathbf{x}_{best} + \gamma(p)(\mathbf{x}_{e_1} - \mathbf{x}_{e_2}) + \delta(\mathbf{c}_E - \mathbf{x}_i) \tag{14}$$

where e_1 and e_2 are two distinct elite indices and δ controls attraction toward the elite centroid. The coefficient γ decreases linearly with search progress:

$$\gamma(p) = \gamma_{max} - (\gamma_{max} - \gamma_{min})p \tag{15}$$

The rank-weighted elite centroid is calculated as:

$$\mathbf{c}_E = \sum_{k=1}^{N_E} w_k \mathbf{x}_{e_k}, \qquad w_k = \frac{k}{\sum_{j=1}^{N_E} j} \tag{16}$$

where the elite solutions are ordered according to fitness so that better-ranked solutions receive greater weights. The decreasing directional coefficient gradually shifts the elite search from broader directional refinement toward more localized exploitation as the function-evaluation budget is consumed. In this way, Equations (14)–(16) connect the progress variable defined in Equation (7), the dynamically constructed elite set from Equations (10) and (11), and the final elite-refinement step.

2.3.5. Candidate Selection and Termination

All candidates generated by the neural, hormonal/cooperative, and elite-refinement mechanisms are repaired to satisfy the parameter bounds and evaluated using the objective function in Equation (6). A greedy replacement rule is applied: a candidate replaces its

current solution only when it yields a lower objective value. The global best solution is subsequently updated from the resulting population. Therefore, the SDM residual RMSE defined in Equation (6) provides the common fitness criterion for all candidate-generation mechanisms described in Equations (12)–(16).

Unlike an iteration-only termination rule, DEC-ACSA uses the number of objective-function evaluations as the computational budget. The search terminates when N_{FE}^{max} is reached. This formulation also enables the proposed algorithm and the comparison methods to be evaluated under an equivalent function-evaluation budget. The same function-evaluation-based termination criterion is retained for all PV benchmarks in the extended validation.

The complete computational sequence of DEC-ACSA is summarized in Algorithm 1, while Figure 2 illustrates the interaction among dynamic grouping, neural search, elite-guided cooperation, and directional elite refinement.

Algorithm 1. Pseudocode of the proposed Dynamic Elite Cooperative Artificial Circulatory System Algorithm (DEC-ACSA)

Input: Objective function, search bounds, and DEC-ACSA parameters
Output: Best solution xbest

Initialize and evaluate population X; set NFE ← N
Identify xbest
while NFE < NFEmax do
    Compute search progress p using Equation (7)
    Compute population diversity D using Equation (8)
    Determine neural and elite ratios using Equations (9) and (10)
    Rank X and form neural, hormonal, and elite groups using Equation (11)
/* Neural search */
    Update neural individuals using Equation (12)
    Repair, evaluate, greedily accept improved candidates, and update NFE
    Refresh the dynamic grouping and elite set
/* Hormonal/cooperative search */
    for each hormonal individual do
        Apply elite-guided cooperation with probability Pc using Equation (11); otherwise apply the ACSA hormonal search mechanism
        Repair, evaluate, greedily accept the candidate, and update NFE
    end for
    Refresh the elite set and compute the rank-weighted elite centroid
/* Elite refinement */
    Update elite individuals using Equations (14)–(16)
    Repair, evaluate, greedily accept improved candidates, and update NFE
    Update xbest
end while
return xbest

https://doi.org/10.3390/engproc2026152004

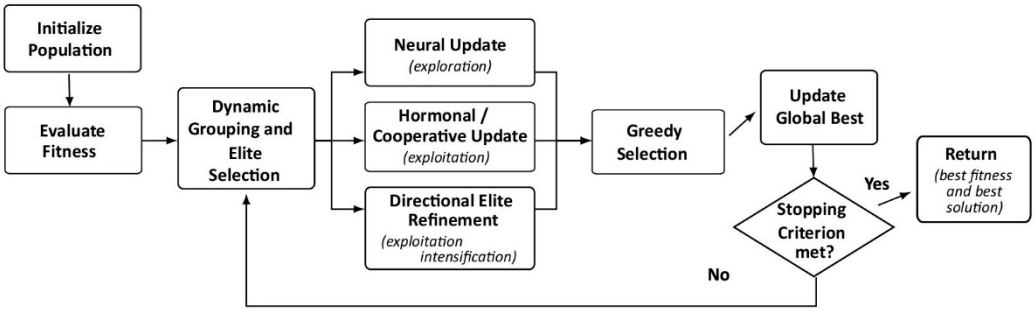


Figure 2. Flowchart of the proposed Dynamic Elite Cooperative Artificial Circulatory System Algorithm (DEC-ACSA).

3. Numerical Results and Discussion

3.1. Computational Setup

The proposed Dynamic Elite Cooperative Artificial Circulatory System Algorithm (DEC-ACSA) was evaluated on four established photovoltaic benchmarks under the Single-Diode Model (SDM): the RTC France solar cell, Photowatt-PWP201, STM6-40/36, and STP6-120/36 PV modules. The optimization problem consists of estimating the five unknown SDM parameters defined in Equation (4), namely the photocurrent (I_{ph}), reverse saturation current (I_s), series resistance (R_s), shunt resistance (R_{sh}), and diode ideality factor (n). The RTC France dataset contains 26 measured I–V points recorded at 33 °C (306.15 K). The three additional module benchmarks extend the validation to different PV technologies and operating temperatures: Photowatt-PWP201 contains 25 I–V points at 45 °C, STM6-40/36 contains 20 points at 51 °C, and STP6-120/36 contains 24 points at 55 °C. Each module comprises 36 series-connected cells (Ns = 36, Np = 1) and is evaluated at an irradiance of 1000 W/m^2.

For RTC France, the original search bounds were retained: $I_{ph} \in [0, 1]$ A, $I_s \in [0, 10^{-6}]$ A, $R_{sh} \in [0, 100]$ Ω, $R_s \in [0, 0.5]$ Ω, and $n \in [1, 2]$. For the three additional modules, the per-cell SDM parameterization introduced in Equations (2) and (3) was used. The bounds were $I_{ph}) \in [0.9\text{Isc}, 1.1\text{Isc}]$ A, $I_s \in [10^{-9}, 10^{-5}]$ A, $R_{sh} \in [0, 100]$ Ω, $R_s \in [0, 0.5]$ Ω, and $n \in [1, 2]$, where Isc is the measured short-circuit-current of the corresponding benchmark. Thus, the physical dataset information and parameter bounds were adapted to each PV device, whereas the optimizer configuration was not retuned for the additional benchmarks.

To ensure a fair comparison, the original ACSA, DEC-ACSA, Genetic Algorithm (GA) [19], Particle Swarm Optimization (PSO) [20], Grey Wolf Optimizer (GWO) [21], and Henry Gas Solubility Optimization (HGSO) [22] were evaluated under identical computational conditions. Each algorithm was independently executed 30 times using a population size of 100 and the same run-wise random seeds. Rather than using the number of iterations as the stopping criterion, all algorithms were limited to an equal budget of 50,100 function evaluations (FEs). The objective function was defined as the residual RMSE of the implicit SDM equation defined in Equation (6). The same algorithm set, population size, FE budget, number of independent runs, and paired-seed protocol were applied to all four benchmarks. Table 1 summarizes the computational configuration adopted throughout this study.

Table 1. Computational configuration used for performance evaluation.

Parameter	RTC France	PWP201	STM6-40/36	STP6-120/36
PV device	Solar cell	PV module	PV module	PV module
Technology	—	Polycrystalline silicon	Monocrystalline silicon	Polycrystalline silicon
Temperature	33 °C (306.15 K)	45 °C (318.15 K)	51 °C (324.15 K)	55 °C (328.15 K)

Table 1. *Cont.*

Parameter	RTC France	PWP201	STM6-40/36	STP6-120/36
Irradiance	—	1000 W/m^2	1000 W/m^2	1000 W/m^2
I–V data points	26	25	20	24
Ns/Np	1/1	36/1	36/1	36/1
Model	SDM	SDM	SDM	SDM
Decision variables	5	5	5	5
Population size	100	100 50,100	100 50,100	100 50,100
Independent runs	30	30	30	30
Objective function	Residual RMSE	Residual RMSE	Residual RMSE	Residual RMSE
Compared algorithms	ACSA, DEC-ACSA, PSO, GWO, GA, HGSO	Same	Same	Same

3.2. Parameter Sensitivity Analysis

A sensitivity analysis was performed for the two principal DEC-ACSA control parameters, Pc and rEmax, which directly govern the activation frequency of the elite-guided cooperative interaction in Equation (11) and the maximum size of the elite subset defined through Equations (10) and (11), respectively. The remaining parameters in Equations (7)–(16) were kept fixed throughout all experiments, whereas Pc and rEmax were examined to quantify the influence of cooperative interaction intensity and elite-set size on the resulting residual RMSE. Pc was varied over {0.70, 0.80, 0.90}, while the maximum elite ratio (rEmax) was varied over {0.20, 0.30, 0.40}. Each configuration was evaluated over 10 independent runs using the same FE budget. Table 2 summarizes the resulting residual RMSE statistics.

Table 2. Sensitivity analysis of the DEC-ACSA control parameters.

P_c	rEmax	Mean RMSE	Std.
0.70	0.20	1.3836×10^{-3}	3.0377×10^{-4}
0.70	0.30	1.2499×10^{-3}	2.3816×10^{-4}
0.70	0.40	1.2200×10^{-3}	3.0516×10^{-4}
0.80	0.20	1.4105×10^{-3}	2.5995×10^{-4}
0.80	0.30	1.2835×10^{-3}	2.0233×10^{-4}
0.80	0.40	1.2501×10^{-3}	1.1725×10^{-4}
0.90	0.20	1.4552×10^{-3}	5.4637×10^{-4}
0.90	0.30	1.3917×10^{-3}	4.8625×10^{-4}
0.90	0.40	1.3365×10^{-3}	3.9441×10^{-4}

The lowest mean residual RMSE was obtained with P_c = 0.70 and rEmax = 0.40; therefore, this configuration was adopted for the subsequent comparative evaluation. The lowest standard deviation was observed for P_c = 0.80 and rEmax = 0.40, indicating that the configuration minimizing the mean error was not necessarily the one producing the smallest run-to-run variation. Importantly, the sensitivity analysis was performed only on the RTC France benchmark. To evaluate transferability without benchmark-specific retuning, the selected configuration (P_c = 0.70 and rEmax = 0.40), together with the remaining DEC-ACSA control parameters, was subsequently kept fixed for the PWP201, STM6-40/36, and STP6-120/36 benchmarks.

3.3. Multi-Benchmark Performance Evaluation

The comparative evaluation was extended from the RTC France solar-cell benchmark to the Photowatt-PWP201, STM6-40/36, and STP6-120/36 PV modules while retaining the same six algorithms, 30 independent paired-seed runs, population size, and 50,100-FE budget. Table 3 summarizes the residual RMSE statistics for all four benchmarks. The residual RMSE corresponds to the objective function defined in Equation (6), so the results directly quantify the ability of each optimizer to identify the five SDM parameters defined in Equation (4) under the common computational protocol.

Table 3. Multi-benchmark statistical comparison of residual RMSE over 30 independent runs. Holm-adjusted *p*-values are reported for paired comparisons against DEC-ACSA within each benchmark.

Benchmark	Algorithm	Best	Mean	Worst	Std.	pHolm vs. DEC-ACSA
RTC France	ACSA	6.395×10^{-3}	3.8694×10^{-2}	1.2064×10^{-1}	2.8919×10^{-2}	9.3132×10^{-9}
	DEC-ACSA	9.863×10^{-4}	1.2514×10^{-3}	2.0376×10^{-3}	2.650×10^{-4}	—
	PSO	9.860×10^{-4}	1.404×10^{-3}	2.448×10^{-3}	4.750×10^{-4}	1.6418×10^{-1}
	GWO	1.193×10^{-3}	2.746×10^{-3}	5.961×10^{-3}	1.214×10^{-3}	9.3132×10^{-9}
	GA	1.319×10^{-3}	1.944×10^{-3}	2.278×10^{-3}	2.710×10^{-4}	9.3132×10^{-9}
	HGSO	2.373×10^{-3}	1.2397×10^{-2}	3.1598×10^{-2}	8.292×10^{-3}	9.3132×10^{-9}
PWP201	ACSA	6.3130×10^{-3}	1.8345×10^{-2}	3.4476×10^{-2}	1.0152×10^{-2}	9.3132×10^{-9}
	DEC-ACSA	2.4260×10^{-3}	2.6560×10^{-3}	3.6450×10^{-3}	2.6700×10^{-4}	—
	PSO	2.4250×10^{-3}	2.8270×10^{-3}	4.0500×10^{-3}	4.2200×10^{-4}	1.6418×10^{-1}
	GWO	2.4650×10^{-3}	4.0200×10^{-3}	1.1174×10^{-2}	1.8600×10^{-3}	2.7932×10^{-5}
	GA	2.6550×10^{-3}	3.0960×10^{-3}	3.6190×10^{-3}	3.0500×10^{-4}	4.9174×10^{-7}
	HGSO	3.6020×10^{-3}	1.2325×10^{-2}	2.7717×10^{-2}	7.3810×10^{-3}	9.3132×10^{-9}
STM6-40/36	ACSA	3.7310×10^{-3}	1.2999×10^{-2}	5.3476×10^{-2}	9.9600×10^{-3}	9.3132×10^{-9}
	DEC-ACSA	1.7300×10^{-3}	2.6470×10^{-3}	3.5200×10^{-3}	4.8800×10^{-4}	—
	PSO	1.8130×10^{-3}	3.1910×10^{-3}	4.6840×10^{-3}	5.2400×10^{-4}	1.5287×10^{-4}
	GWO	2.2380×10^{-3}	5.6530×10^{-3}	1.4942×10^{-2}	2.2530×10^{-3}	1.1176×10^{-8}
	GA	2.5240×10^{-3}	3.5960×10^{-3}	4.2850×10^{-3}	4.6400×10^{-4}	9.3132×10^{-9}
	HGSO	4.3530×10^{-3}	1.1911×10^{-2}	2.5504×10^{-2}	5.9630×10^{-3}	9.3132×10^{-9}
STP6-120/36	ACSA	1.8913×10^{-2}	4.3251×10^{-2}	1.4741×10^{-1}	3.0054×10^{-2}	1.6764×10^{-8}
	DEC-ACSA	1.6602×10^{-2}	1.8108×10^{-2}	2.0687×10^{-2}	1.2940×10^{-3}	—
	PSO	1.6717×10^{-2}	7.0528×10^{-2}	3.1234×10^{-1}	1.1008×10^{-1}	2.6885×10^{-5}
	GWO	1.7883×10^{-2}	8.0561×10^{-2}	3.9516×10^{-1}	1.2770×10^{-1}	1.8626×10^{-8}
	GA	1.8313×10^{-2}	2.3262×10^{-2}	2.7856×10^{-2}	2.2190×10^{-3}	9.3132×10^{-9}
	HGSO	1.8828×10^{-2}	7.1549×10^{-2}	2.6532×10^{-1}	6.6241×10^{-2}	9.3132×10^{-9}

On RTC France, DEC-ACSA retained the performance reported in the first revision, with a mean residual RMSE of 1.2514×10^{-3} and a standard deviation of 2.65×10^{-4}. Although PSO produced a marginally lower best value (9.860×10^{-4} versus 9.863×10^{-4}), the paired difference between DEC-ACSA and PSO remained non-significant after Holm correction (pHolm = 0.1642). DEC-ACSA was significantly different from ACSA, GWO, GA, and HGSO.

The additional benchmarks show that the stability improvement is not restricted to RTC France. For PWP201, DEC-ACSA achieved a mean residual RMSE of 2.656×10^{-3} with a standard deviation of 2.67×10^{-4}, compared with $1.8345 \times 10^{-2} \pm 1.0152 \times 10^{-2}$ for ACSA. PSO produced a nearly identical best value, and its paired difference from DEC-ACSA was again not significant (pHolm = 0.1642), whereas the differences from ACSA, GWO, GA, and HGSO were significant. For STM6-40/36, DEC-ACSA obtained the lowest mean residual RMSE (2.647×10^{-3}) and a standard deviation of 4.88×10^{-4};

all five pairwise comparisons were significant after Holm correction. On STP6-120/36, DEC-ACSA achieved a mean residual RMSE of 1.8108×10^{-2} with a standard deviation of 1.294×10^{-3}, substantially below the mean values obtained by ACSA, PSO, GWO, GA, and HGSO; all pairwise differences were significant after correction.

Because identical run-wise seeds were used, the statistical analysis was performed separately within each benchmark using the paired Wilcoxon signed-rank test followed by Holm correction. This benchmark-wise procedure avoids pooling errors from PV systems with different current scales and operating characteristics. Across the three additional modules, DEC-ACSA outperformed the original ACSA in 30/30 paired runs for PWP201, 30/30 for STM6-40/36, and 29/30 for STP6-120/36. These results provide additional evidence that the reduction in run-to-run variability observed on RTC France transfers to different PV module datasets without benchmark-specific retuning.

Figures 3 and 4 provide complementary visual comparisons of the optimization performance across the four benchmarks. Figure 3 presents the FE-aligned mean convergence curves, whereas Figure 4 shows the distributions of the final residual RMSE values over 30 independent runs. Convergence is plotted against function evaluations rather than nominal iterations so that the common computational budget is preserved in the visual comparison.

As shown in Figure 3, DEC-ACSA exhibits a more stable convergence pattern across the four PV benchmarks, generally reaching low residual RMSE levels without the pronounced late-run variability observed for some comparison methods. This behavior is consistent with the reduced run-to-run variability reported in Table 3 and suggests that the proposed cooperative mechanisms improve the convergence stability of the baseline ACSA.

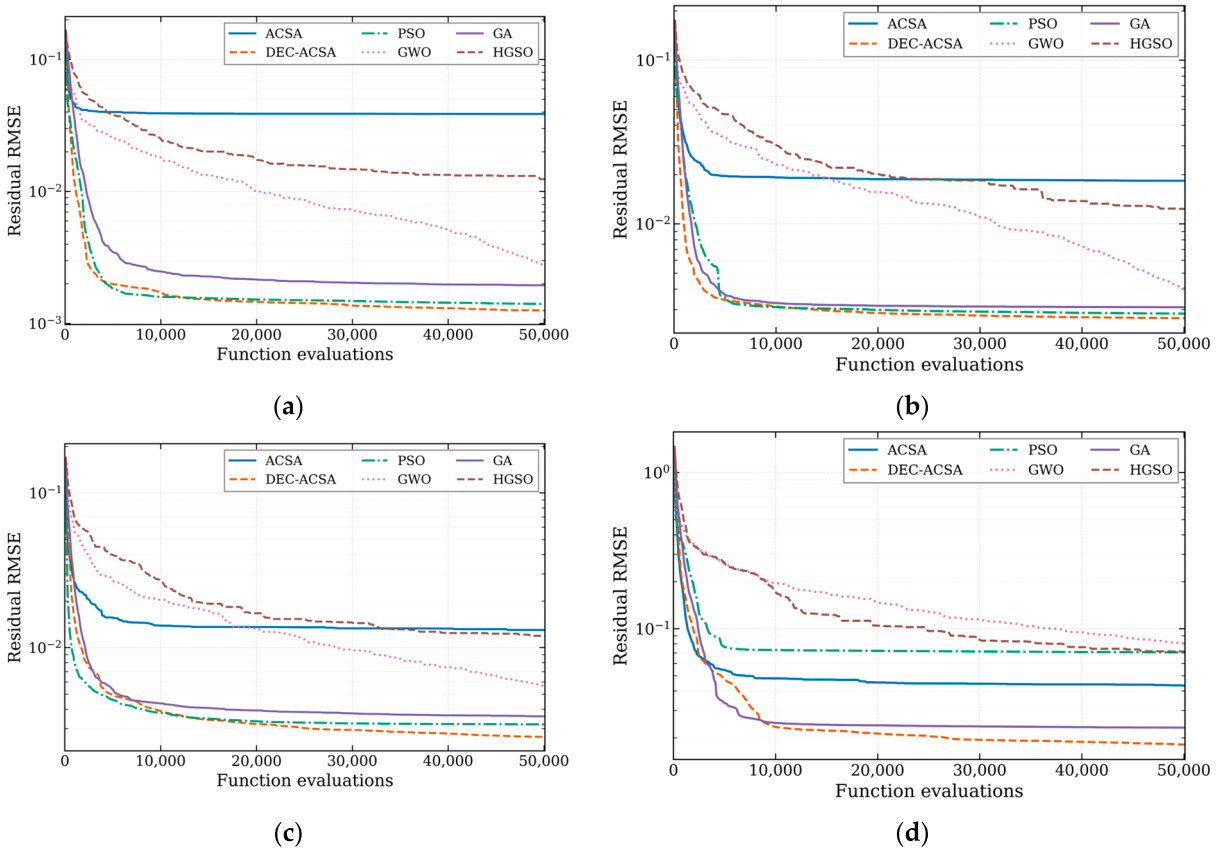


Figure 3. Mean conve. ence curves over 30 independent runs as a function of the number of function evaluations for (**a**) RTC France, (**b**) PWP201, (**c**) STM6-40/36, and (**d**) STP6-120/36.

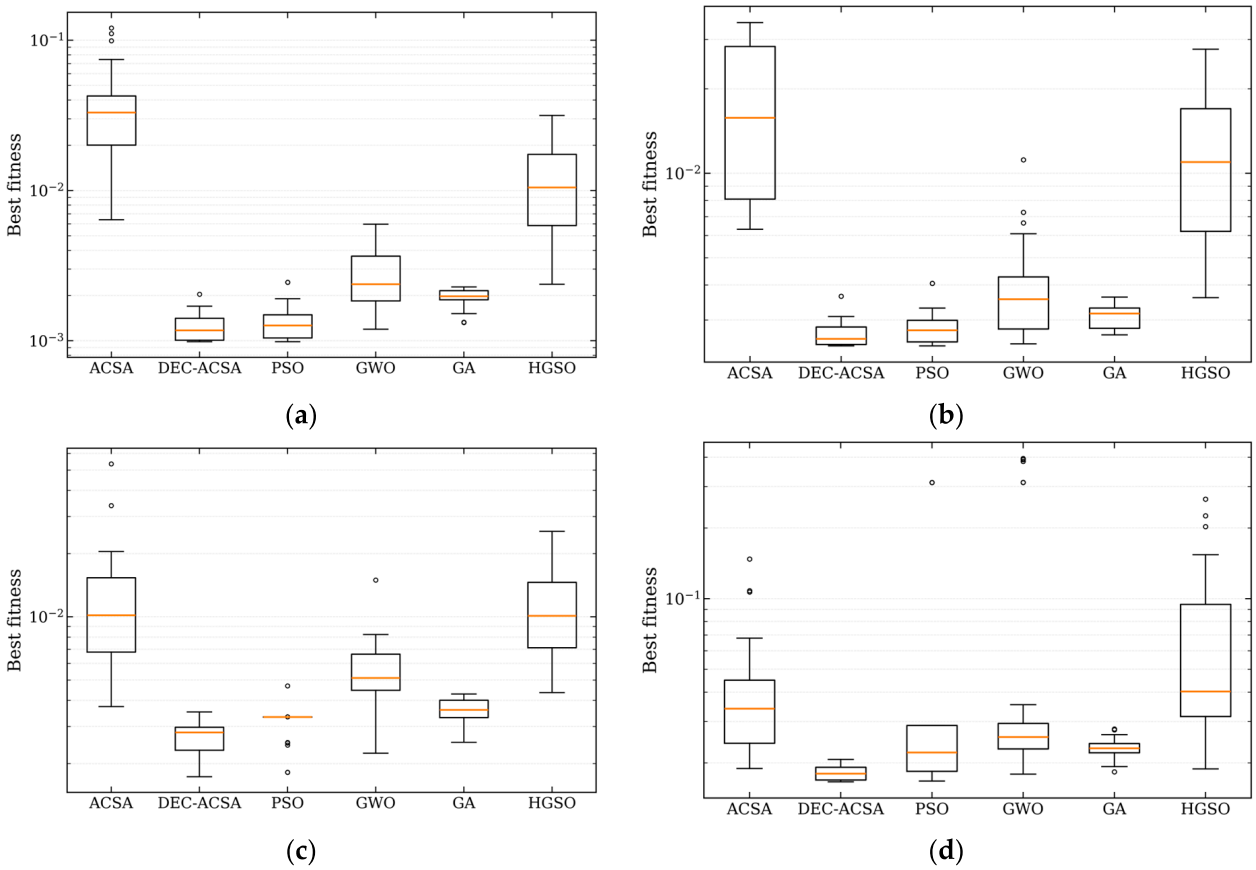


Figure 4. Distribution of the final residual RMSE values over 30 independent runs for (**a**) RTC France, (**b**) PWP201, (**c**) STM6-40/36, and (**d**) STP6-120/36.

The boxplots in Figure 4 further support the statistical findings in Table 3. DEC-ACSA shows compact final-RMSE distributions across the four benchmarks, particularly in comparison with the original ACSA, indicating reduced sensitivity to run-wise stochastic variation. The overlap between DEC-ACSA and PSO on RTC France and PWP201 is also consistent with the non-significant pairwise differences obtained for these two benchmarks.

3.4. Photovoltaic Parameter Estimation and I–V Reconstruction

To complement the optimization-domain assessment, the parameter vectors obtained from the best residual-RMSE runs were used to reconstruct the I–V characteristics by numerically solving the implicit SDM relation in Equations (2) and (3). The five quantities reported in Table 4 therefore correspond directly to the decision variables defined in Equation (4), while the reconstruction RMSE provides an independent physical-domain measure of agreement between the identified SDM and the measured I–V data.

For the additional module benchmarks, the best DEC-ACSA solutions yielded I–V reconstruction RMSE values of 2.149×10^{-3} for PWP201, 1.723×10^{-3} for STM6-40/36, and 1.4407×10^{-2} for STP6-120/36. The corresponding mean reconstruction RMSE values across 30 runs were 2.387×10^{-3}, 2.637×10^{-3}, and 1.6296×10^{-2}, respectively. The close agreement between the optimization-domain residual RMSE and the reconstructed I–V behavior confirms that the parameter vectors identified through Equation (6) also reproduce the measured electrical characteristics when substituted into the implicit SDM equations.

Figure 5 shows the measured and reconstructed I–V characteristics for all four systems. This presentation permits direct visual assessment of the fitted curves across the original solar-cell benchmark and the three additional PV modules while avoiding separate, repetitive figures for each dataset.

Table 4. Best SDM parameters and corresponding I–V reconstruction RMSE for the four PV benchmarks. For the module datasets, R_s and R_{sh} are reported on a per-cell basis.

Benchmark	Algorithm	I_{ph} (A)	I_s (A)	R_{sh} (Ω)	R_s (Ω)	n
RTC France	ACSA	0.7579	1.5224×10^{-7}	42.9450	0.0363	1.4103
	DEC-ACSA	0.7608	3.2012×10^{-7}	53.2060	0.0364	1.4803
	PSO	0.7608	3.2309×10^{-7}	53.7250	0.0364	1.4812
	GWO	0.7602	4.4787×10^{-7}	71.5600	0.0351	1.5148
	GA	0.7598	4.3105×10^{-7}	79.6740	0.0356	1.5106
	HGSO	0.7613	6.8356×10^{-7}	68.0940	0.0332	1.5613
PWP201	ACSA	1.0218	1.0000×10^{-6}	25.3397	0.0366	1.2368
	DEC-ACSA	1.0304	4.0000×10^{-6}	27.8953	0.0333	1.3532
	PSO	1.0304	4.0000×10^{-6}	27.7775	0.0333	1.3528
	GWO	1.0310	4.0000×10^{-6}	26.9480	0.0330	1.3612
	GA	1.0276	5.0000×10^{-6}	52.3705	0.0323	1.3908
	HGSO	1.0301	7.0000×10^{-6}	47.0730	0.0308	1.4371
STM6-40/36	ACSA	1.6590	3.0000×10^{-6}	18.4430	0.0021	1.5743
	DEC-ACSA	1.6640	2.0000×10^{-6}	15.8100	0.0043	1.5183
	PSO	1.6631	2.0000×10^{-6}	17.2285	0.0036	1.5420
	GWO	1.6615	3.0000×10^{-6}	21.1420	0.0030	1.5734
	GA	1.6599	3.0000×10^{-6}	22.1067	0.0032	1.5692
	HGSO	1.6577	7.0000×10^{-6}	58.5982	1.9000×10^{-5}	1.6912
STP6-120/36	ACSA	7.4698	3.0000×10^{-6}	22.4002	0.0044	1.2823
	DEC-ACSA	7.4735	2.0000×10^{-6}	20.5582	0.0046	1.2592
	PSO	7.4678	3.0000×10^{-6}	47.9391	0.0045	1.2727
	GWO	7.4684	2.0000×10^{-6}	27.1387	0.0048	1.2401
	GA	7.4735	4.0000×10^{-6}	40.2294	0.0043	1.2987
	HGSO	7.4609	2.0000×10^{-6}	49.9084	0.0046	1.2587

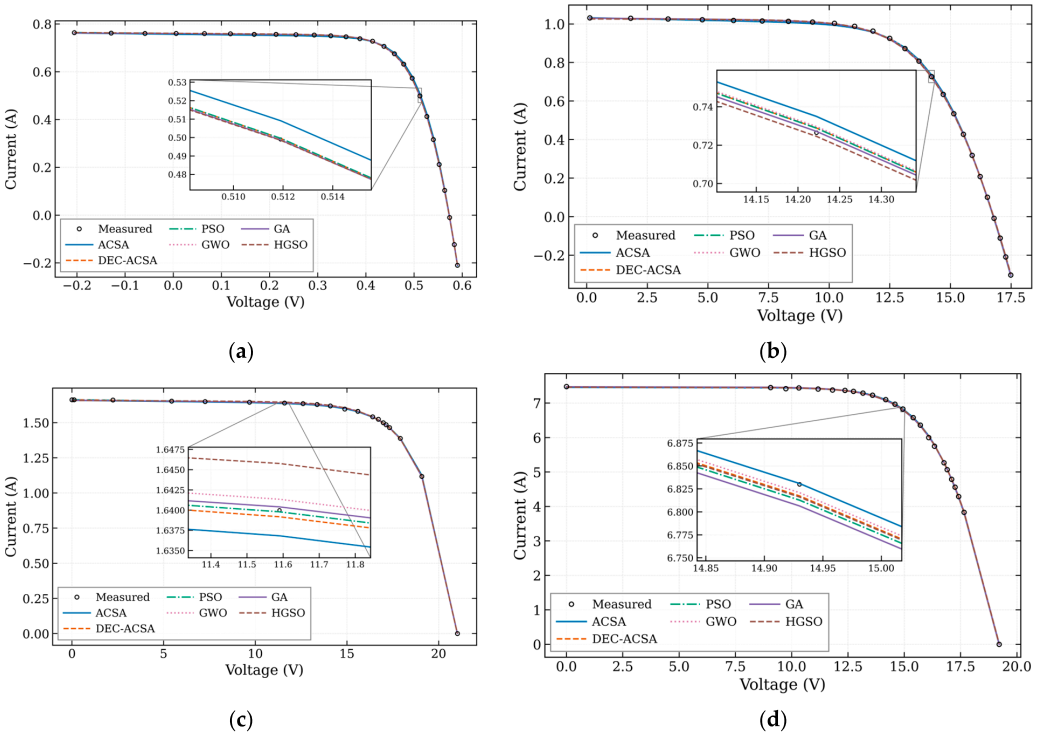


Figure 5. Measured and reconstructed I–V characteristics obtained using the best DEC-ACSA solutions for (**a**) RTC France, (**b**) PWP201, (**c**) STM6-40/36, and (**d**) STP6-120/36.

As illustrated in Figure 5, the I–V curves reconstructed using the best DEC-ACSA parameter sets closely follow the measured data for all four PV systems. This agreement across both the RTC France cell and the three additional PV modules provides a physical-domain confirmation that the low residual RMSE values correspond to accurate reproduction of the measured electrical characteristics.

3.5. Computational Cost

Since all algorithms used the same budget of 50,100 function evaluations, execution time was also recorded to assess the computational burden. The mean runtimes were 16.23 s for HGSO, 17.01 s for PSO, 17.25 s for GWO, 17.54 s for ACSA, 20.12 s for DEC-ACSA, and 20.98 s for GA. Thus, the additional population-management operations in DEC-ACSA resulted in a moderate increase in execution time relative to the original ACSA, while the number of objective-function evaluations remained identical for all methods. The same pattern was observed on the additional PV modules. DEC-ACSA required mean runtimes of 20.85 s, 17.83 s, and 20.08 s for PWP201, STM6-40/36, and STP6-120/36, respectively, compared with 18.35 s, 15.09 s, and 17.39 s for the corresponding ACSA runs. Nevertheless, all algorithms used the same budget of 50,100 FEs on every benchmark. Thus, the extended validation indicates that the improved stability of DEC-ACSA is accompanied by a moderate runtime overhead attributable to its dynamic grouping and elite-management operations rather than to a larger number of objective-function evaluations.

3.6. Discussion

The observed differences between ACSA and DEC-ACSA are consistent with the changes introduced in the population-update mechanism. In DEC-ACSA, diversity-aware dynamic grouping, elite-guided cooperative interaction, and directional elite refinement allow information from a dynamically updated set of high-quality solutions to influence the search rather than relying predominantly on a single best solution. The numerical results indicate that this modification is associated with lower run-to-run variability and lower residual RMSE than the original ACSA under the same function-evaluation budget.

The extended validation shows that this behavior is not restricted to the RTC France solar-cell benchmark. With the sensitivity-selected DEC-ACSA configuration kept unchanged, the algorithm achieved lower mean residual RMSE than the original ACSA on PWP201, STM6-40/36, and STP6-120/36, in addition to RTC France. The corresponding run-to-run variability was also substantially reduced relative to ACSA across the four datasets. This is particularly relevant because the additional benchmarks represent PV modules with different electrical characteristics and operating temperatures, and no benchmark-specific retuning of the DEC-ACSA control parameters was performed.

The comparison with the other metaheuristic algorithms further indicates that the relative performance of DEC-ACSA depends on the benchmark. On RTC France, DEC-ACSA achieved a mean residual RMSE of 1.2514×10^{-3}, compared with 1.404×10^{-3} for PSO, but the paired difference was not statistically significant after Holm correction (pHolm = 0.1642). A similar pattern was observed on PWP201, where DEC-ACSA and PSO produced closely matched performance and the corrected difference was again not significant. In contrast, on STM6-40/36 and STP6-120/36, DEC-ACSA achieved the lowest mean residual RMSE among the evaluated methods and its pairwise differences from all five comparison algorithms were statistically significant after Holm correction. These results therefore support improved robustness across the investigated PV systems while avoiding a universal claim of superiority over PSO.

The physical-domain reconstruction results are consistent with the optimization-domain findings. The parameter vectors defined in Equation (4), obtained by mini-

mizing the residual RMSE in Equation (6), produced reconstructed I–V characteristics that closely followed the measured data when substituted into the SDM relations in Equations (2) and (3). The best DEC-ACSA solutions yielded I–V reconstruction RMSE values of 1.0406×10^{-3} for RTC France, 2.149×10^{-3} for PWP201, 1.723×10^{-3} for STM6-40/36, and 1.4407×10^{-2} for STP6-120/36. The differences in the absolute RMSE scale across datasets should be interpreted in relation to the different current ranges and electrical characteristics of the corresponding PV devices rather than as direct cross-dataset performance rankings.

The additional population-management operations introduce a moderate computational overhead. For RTC France, the mean runtime increased from 17.54 s for ACSA to 20.12 s for DEC-ACSA. The same pattern was observed for PWP201 (18.35 s versus 20.85 s), STM6-40/36 (15.09 s versus 17.83 s), and STP6-120/36 (17.39 s versus 20.08 s). However, all methods were restricted to the same 50,100 function evaluations on every benchmark. The runtime increase should therefore be interpreted as the computational cost of the additional dynamic grouping and elite-management operations rather than as a consequence of a larger objective-function evaluation budget.

Overall, the multi-benchmark results strengthen the evidence that the DEC modification improves the convergence stability of the baseline ACSA beyond a single PV dataset. Nevertheless, the present validation remains limited to the SDM and to four established cell/module benchmarks under fixed measurement conditions. The results therefore support transferability across the investigated PV systems, but broader generalization to other diode models, PV technologies, irradiance levels, or real-world time-varying operating conditions requires further study.

4. Conclusions

This study presented a Dynamic Elite Cooperative Artificial Circulatory System Algorithm (DEC-ACSA) for photovoltaic parameter identification based on the Single-Diode Model (SDM). By incorporating diversity-aware dynamic population grouping, elite-guided cooperative interaction, and directional elite refinement into the original ACSA framework, the proposed approach aims to improve convergence stability and the utilization of high-quality population information during the search process.

The numerical evaluation was extended from the RTC France solar cell to three additional PV module benchmarks, namely PWP201, STM6-40/36, and STP6-120/36. Importantly, the DEC-ACSA parameter configuration selected through the RTC France sensitivity analysis (P_c = 0.70 and rEmax = 0.40) was transferred unchanged to the additional benchmarks, thereby avoiding benchmark-specific retuning. Across 30 independent runs under a common budget of 50,100 function evaluations, DEC-ACSA obtained mean residual RMSE values of 1.2514×10^{-3}, 2.656×10^{-3}, 2.647×10^{-3}, and 1.8108×10^{-2} for RTC France, PWP201, STM6-40/36, and STP6-120/36, respectively. In each case, the mean residual RMSE was lower than that of the original ACSA, with substantially reduced run-to-run variability.

Comparisons with PSO, GWO, GA, and HGSO showed that DEC-ACSA achieved the lowest mean residual RMSE among the evaluated methods on all four benchmarks. However, the statistical results also indicate that this numerical advantage should be interpreted carefully: the difference between DEC-ACSA and PSO was not statistically significant after Holm correction on RTC France and PWP201, whereas statistically significant differences were obtained against all comparison algorithms on STM6-40/36 and STP6-120/36. The I–V reconstruction analysis further confirmed that the identified SDM parameter sets reproduced the measured electrical characteristics across all four systems.

https://doi.org/10.3390/engproc2026152004

The improved optimization stability was accompanied by a moderate runtime increase relative to the original ACSA, while the function-evaluation budget remained identical for all methods and datasets. Taken together, the results provide stronger evidence that the DEC framework can improve the robustness of ACSA across different PV cell/module benchmarks rather than only on the original RTC France dataset. At the same time, the conclusions are restricted to the four investigated SDM benchmarks and the operating conditions represented by their measured I–V data.

Future work will focus on extending the proposed approach to more complex photovoltaic models, including the Double-Diode Model, and on evaluating its behavior under broader irradiance and temperature conditions as well as additional PV technologies and real-world operating data. Such studies will be necessary to assess the generalizability of the observed stability improvements beyond the benchmark conditions considered here.

Author Contributions: Conceptualization and methodology, N.Ö. and I.B.G.; software and validation, N.Ö.; formal analysis, N.Ö. and I.B.G.; writing—original draft preparation, N.Ö.; writing—review and editing, N.Ö. and I.B.G.; visualization, N.Ö. All authors have read and agreed to the published version of the manuscript.

Funding: This research received no external funding.

Institutional Review Board Statement: Not applicable.

Informed Consent Statement: Not applicable.

Data Availability Statement: The data and source code supporting the findings of this study are available from the corresponding author upon reasonable request.

Acknowledgments: During the preparation of this manuscript, the authors used ChatGPT (GPT-5.6, OpenAI) for language editing and code refinement. All AI-assisted content was critically reviewed and verified by the authors, who take full responsibility for the final manuscript.

Conflicts of Interest: The authors declare no conflicts of interest.

References

1. Ali, A.O.; Elgohr, A.T.; El-Mahdy, M.H.; Zohir, H.M.; Emam, A.Z.; Mostafa, M.G.; Al-Razgan, M.; Kasem, H.M.; Elhadidy, M.S. Advancements in photovoltaic technology: A comprehensive review of recent advances and future prospects. *Energy Convers. Manag. X* **2025**, *26*, 100952. [CrossRef]
2. Ćalasan, M.; Vujošević, S.; Micev, M.; Radonjić, I.; Petronijević, M. Two- and three-diode models for solar cells: The impact of series resistance repositioning on performance and accuracy. *Energy* **2026**, *355*, 141152. [CrossRef]
3. Tanguturi, S.; Injeti, S.K.; Maineni, V.; Nuvvula, R.S.S.; Tangi, S. An Enhanced Polar Light Optimizer with SD-RFAT refinement for efficient parameter estimation of solar PV models. *Results Control Optim.* **2026**, *24*, 100720. [CrossRef]
4. Sharma, A.; Sharma, A.; Averbukh, M.; Jately, V.; Rajput, S.; Azzopardi, B.; Lim, W.H. Performance investigation of state-of-the-art metaheuristic techniques for parameter extraction of solar cells/module. *Sci. Rep.* **2023**, *13*, 11134. [CrossRef] [PubMed]
5. Almutairi, S.Z.; Shaheen, A.M. A novel kangaroo escape optimizer for parameter estimation of solar photovoltaic cells/modules via one, two and three-diode equivalent circuit modeling. *Sci. Rep.* **2025**, *15*, 32669. [CrossRef] [PubMed]
6. Yousri, D.; Elaziz, M.A.; Oliva, D.; Abualigah, L.; Al-Qaness, M.A.A.; Ewees, A.A. Reliable applied objective for identifying simple and detailed photovoltaic models using modern metaheuristics: Comparative study. *Energy Convers. Manag.* **2020**, *223*, 113279. [CrossRef]
7. Gu, Z.; Xiong, G.; Fu, X. Parameter Extraction of Solar Photovoltaic Cell and Module Models with Metaheuristic Algorithms: A Review. *Sustainability* **2023**, *15*, 3312. [CrossRef]
8. Almodfer, R.; Mudhsh, M.; Alshathri, S.; Yousri, D.; Abualigah, L.; Hassan, O.F.; Elaziz, M.A. Chaotic honey badger algorithm for single and double photovoltaic cell/module. *Front. Energy Res.* **2022**, *10*, 1011887. [CrossRef]
9. Rathod, A.A.; Subramanian, B. Efficient approach for optimal parameter estimation of PV using Pelican Optimization Algorithm. *Cogent Eng.* **2024**, *11*, 2380805. [CrossRef]
10. Bennagi, A.; AlHousrya, O.; Cotfas, D.T.; Cotfas, P.A. Parameter extraction of photovoltaic cells and panels using a PID-Based metaheuristic algorithm. *Appl. Sci.* **2025**, *15*, 7403. [CrossRef]

11. Almabrouk, A.A.M.; Avci, S.A.; Rahebi, J. Parameter Estimation in photovoltaic systems using a hybrid Bat and crow metaheuristic algorithm. *Sci. Rep.* **2026**, *16*, 4670. [CrossRef] [PubMed]
12. Özcan, N.; Gürsoy-Demir, H. Levy Flight-Augmented Artificial Circulatory System Algorithm for optimal PID tuning in DC motor control. *AEU-Int. J. Electron. Commun.* **2025**, *204*, 156101. [CrossRef]
13. Ramadan, A.; Kamel, S.; Hussein, M.M.; Hassan, M.H. A New Application of Chaos Game Optimization Algorithm for Parameters Extraction of Three Diode Photovoltaic Model. *IEEE Access* **2021**, *9*, 51582–51594. [CrossRef]
14. Saleh Alluhaidan, A.; Salama AbdElminaam, D.; Ghanim, T.M.; El-Rahman, S.A.; Farahat, I.S.; Al Tawil, A.; Alkady, Y.; Elashmawi, W.H. Refined photovoltaic parameters estimation via an improved Sinh Cosh Optimizer with trigonometric operators. *Sci. Rep.* **2025**, *15*, 4481. [CrossRef] [PubMed]
15. Abdel-Basset, M.; Mohamed, R.; El-Fergany, A.; Abouhawwash, M.; Askar, S.S. Parameters Identification of PV Triple-Diode model using improved Generalized normal distribution algorithm. *Mathematics* **2021**, *9*, 995. [CrossRef]
16. Almutairi, S.Z.; Shaheen, A.M. Improved Black-Winged KITE algorithm for sustainable photovoltaic energy modeling and accurate parameter estimation. *Sustainability* **2026**, *18*, 731. [CrossRef]
17. Özcan, N.; Utku, S.; Berber, T. Artificial Circulation System Algorithm: A Novel Bio-Inspired Algorithm. *Comput. Model. Eng. Sci.* **2025**, *142*, 635–663. [CrossRef]
18. Easwarakhanthan, T.; Bottin, J.; Bouhouch, I.; Boutrit, C. Nonlinear Minimization Algorithm for Determining the Solar Cell Parameters with Microcomputers. *Int. J. Sustain. Energy* **1986**, *4*, 1–12. [CrossRef]
19. Holland, J.H. Genetic algorithms. *Sci. Am.* **1992**, *267*, 66–72. [CrossRef]
20. Eberhart, R.; Kennedy, J. A new optimizer using particle swarm theory. In Proceedings of the Sixth International Symposium on Micro Machine and Human Science, Nagoya, Japan, 4–6 October 1995; pp. 39–43. [CrossRef]
21. Mirjalili, S.; Mirjalili, S.M.; Lewis, A. Grey Wolf Optimizer. *Adv. Eng. Softw.* **2014**, *69*, 46–61. [CrossRef]
22. Hashim, F.A.; Houssein, E.H.; Mabrouk, M.S.; Al-Atabany, W.; Mirjalili, S. Henry gas solubility optimization: A novel physics-based algorithm. *Future Gener. Comput. Syst.* **2019**, *101*, 646–667. [CrossRef]

Disclaimer/Publisher's Note: The statements, opinions and data contained in all publications are solely those of the individual author(s) and contributor(s) and not of MDPI and/or the editor(s). MDPI and/or the editor(s) disclaim responsibility for any injury to people or property resulting from any ideas, methods, instructions or products referred to in the content.